Visualization of developmental processes by extrusion in space time

Mark Hammel and Przemyslaw Prusinkiewicz
Department of Computer Science
University of Calgary
Calgary, Alberta, Canada T2N 1N4
e-mail: hammel|pwp@cpsc.ucalgary.ca

From *Proceeding of Graphics Interface '96*, pages 246–258, May 1996
Held in Toronto, Ontario, 21-24 May 1996

Visualization of developmental processes by extrusion in space-time

Mark Hammel and Przemyslaw Prusinkiewicz
Department of Computer Science
University of Calgary
Calgary, Alberta, Canada T2N 1N4
e-mail: hammel|pwp@cpsc.ucalgary.ca

Abstract

Developmental processes in nature may involve complex changes in the topology, shape, and patterns of growing structures. Processes taking place in one or two dimensions can be visualized as objects in three-dimensional space, obtained by extruding the growing structures along a line or curve representing the progress of time. In this paper, we extend the notion of L-systems with turtle interpretation to facilitate the construction of such objects. This extension is based on the interpretation of the entire derivation graph generated by an L-system, as opposed to the interpretation of individual words. We illustrate the proposed method by applying it to visualize the development of compound leaves, a sea shell with a pigmentation pattern, and a filamentous bacteria. In addition to serving as visualization examples, these models are of interest on their own. The sea shell model uses an L-system to express a reaction-diffusion process, thus relating these two models of morphogenesis. The model of bacteria, which is also of the reaction-diffusion type, sheds new light on one of the basic problems of morphogenesis, the formation of equally spaced organs in a developing medium.

Keywords: L-system, fractal, plant, sea shell, generative modeling, reaction-diffusion, simulation, visualization.

1 Introduction

Animation provides a natural means of visualizing developmental processes, yet it may be unsuitable as a medium of presentation, for example in printed documents. Consequently, developmental processes are often illustrated using sequences of images that represent selected stages of development. Unfortunately, this approach fails to convey the gradual progression of forms and patterns. In addition, sequences of images make it difficult to perceive differential aspects of development, such as the growth rates of branches in plant models.

We describe a partial solution to this problem, suitable for illustrating the development of one- and two-dimensional structures and patterns. The key idea is to visualize a developmental process as a three-dimensional object, obtained by extruding the growing structure along an axis representing the progress of time.

The concept of representing developmental processes as objects in space-time is certainly not new. In essence, any three-dimensional plot of a function $y = f(x, t)$, where the variable t represents time and the dependent variable y is interpreted as height, color, or both [32, Chapter 1], can be regarded as an "object in space-time." In the context of biological modeling, space-time plots have been widely used by Meinhardt to illustrate the gradual changes in morphogen distribution postulated by reaction-diffusion models [13]. In particular, he applied such plots to model the pigmentation patterns of sea shells as space-time records of morphogen distribution along the shell edge [15, 16]. The origins of process visualization using space-time objects can also be traced to modeling techniques based on sweeping time-varying planar shapes along a line or a curve ("generative modeling" [25, 26]).

To render a space-time object, its boundary representation can be formed by connecting vertices of consecutive cross-sections that capture the growing structure at discrete time intervals. In contrast to the basic extrusion method, where the process of finding and connecting corresponding vertices is straightforward (for example, see [30]), in growing structures one must take into account changes in the topology and the number of vertices between cross-sections. In this paper, we focus on developmental processes modeled using L-systems. The connections between vertices and the resulting boundary polygons can then be conveniently expressed in terms of L-system productions.

The relationship between L-systems and extrusion has implications that go beyond visualization of developmental processes as abstract space-time objects. In particular, extrusion extends the range of natural phenomena that can be modeled using L-systems to sea shells with pigmentation patterns. The possibility of modeling sea shells using L-systems reveals a relationship between L-systems and reaction-diffusion models, which until now were viewed

as competing rather than complementary theories of morphogenesis. In addition, the integration of L-systems and reaction-diffusion models provides a framework for considering reaction-diffusion processes in growing media, as opposed to the static media usually considered (c.f. [13, 28]).

The paper is organized as follows. In Sections 2 and 3 we summarize background information regarding parametric L-systems with turtle interpretation. On this basis, in Section 4 we define the extruded interpretation of L-systems, and in Section 5 we illustrate it using selected mathematical and biological examples. In Section 6, we use space-time objects generated by L-systems to visualize numerical solutions to a class of partial-differential equations. On this basis, we present models of the sea shell *Nautilus pompilius* and of heterocyst formation and spacing in a growing filament of the bacteria *Anabaena catenula*, which establish a conceptual link between L-systems and reaction-diffusion models. Finally, in Section 7 we summarize the results of this paper, and present a list of problems open for further study.

2 Parametric L-systems

An extensive exposition of parametric L-systems is given in [23]. Aspects of this formalism essential to the visualization of developmental processes using space-time objects are presented below.

An L-system is a parallel rewriting system operating on strings of symbols with associated parameters. These strings are also called *parametric words*, and their elements are called *modules*. A parametric word may represent a linear or branching structure; branches are enclosed in well-nested pairs of brackets. At the heart of an L-system is its set of *productions*, or rewriting rules for replacing a *predecessor* module with zero, one, or more *successor* modules. In the class of deterministic context-sensitive parametric L-systems considered in this paper, productions have the format:

$$id : lc < pred > rc : cond \rightarrow succ \tag{1}$$

where id is the production identifier (label), lc, $pred$, and rc are the left context, the strict predecessor, and the right context, $cond$ is the condition, and $succ$ is the successor. The strict predecessor and successor are the only mandatory fields. A production can be applied to a module if it appears in the proper context, and the condition evaluates to *true*. For example, the production

$$\begin{aligned} p: \quad & A(x) < B(y) > C(z) : x + y + z > 10 \\ & \rightarrow E((x+y)/2)[F((y+z)/2)]G \end{aligned} \tag{2}$$

can be applied to the module $B(5)$ in the parametric word

$$\cdots A(4)B(5)C(6)\cdots \tag{3}$$

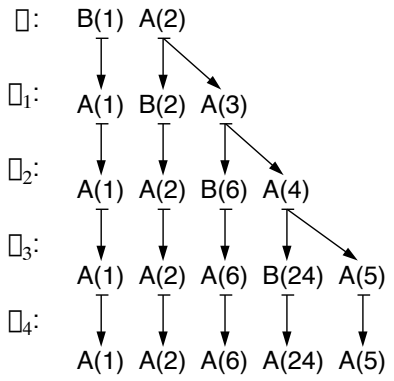

Figure 1: Derivation graph for the developmental sequence generated by the parametric L-system specified in Equation (5)

because the sequence of letters A, B, C in production (2) is the same as in parametric word (3), and the condition

$$4 + 5 + 6 > 10 \tag{4}$$

is true. As a result of applying this production, the module $B(5)$ will be replaced by the parametric word $E(4.5)[F(5.5)]G$.

If a module a is replaced by a parametric word χ as the result of a production application in an L-system $\mathcal{G}$, we write $a \mapsto \chi$. Given a parametric word $\mu = a_1 a_2 \ldots a_n$, we say that the word $\nu = \chi_1 \chi_2 \ldots \chi_n$ is derived from μ in a single *derivation step* (or *directly*), and write $\mu \Longrightarrow \nu$, if and only if $a_i \mapsto \chi_i$ for all $i = 1, 2, \ldots, n$. By convention, if no production explicitly included in the production set applies to a module a_j, we replace it by itself: $a_j \mapsto a_j$. Given a predefined word ω called the *axiom* of L-system $\mathcal{G}$, a sequence of words $S = \mu_0, \mu_1, \mu_2, \ldots$ such that $\mu_0 = \omega$ and $\mu_0 \Longrightarrow \mu_1 \Longrightarrow \mu_2 \Longrightarrow \cdots$ is called the *developmental sequence* generated by $\mathcal{G}$.

For example, Figure 1 shows the developmental sequence S generated by the following L-system:

$$\begin{aligned} \omega &: \quad B(1)A(2) \\ p_1 &: \quad B(x) < A(y) : y < 5 \\ &\qquad \rightarrow B(x * y)A(y+1) \\ p_2 &: \quad B(x) \quad \rightarrow A(x) \end{aligned} \tag{5}$$

This figure is an example of a *derivation graph* [8, Section 2.4]. A derivation graph lists consecutive elements of the developmental sequence generated by $\mathcal{G}$, and records all production applications by relating predecessor modules in a string μ_i to their respective successors in the string μ_{i+1}. Unlike derivation trees for Chomsky grammars, which are meaningful only in the context-free case, the L-system graphs can also depict context-sensitive deriva-

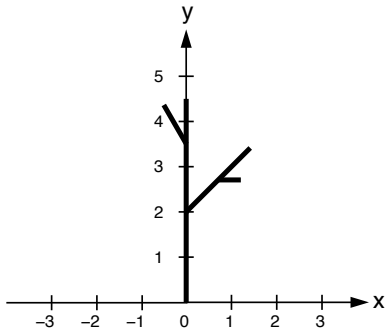

Figure 2: Example of the turtle interpretation of a parametric word. The default length of lines represented by symbol F without parameters is 1, and the default magnitude of angles represented by symbols $+$ and $-$ is 45°.

tions, since the context of each module is clearly indicated by its position in the string.

3 Turtle interpretation of L-systems

The strings generated by L-systems can be interpreted geometrically using *turtle interpretation* [20, 27] extended to parametric words [23]. In a nutshell, the interpreted string is scanned sequentially from left to right, and the modules act as commands that control a LOGO-style turtle. The interpreted modules considered in this paper are listed below:

$F(s)$ Move forward a step of length s and draw a line segment from the original position to the new position of the turtle.

$f(s)$ Move forward a step of length s without drawing a line (the line is considered "invisible").

$+(\theta)$ Turn left by angle θ.

$-(\theta)$ Turn right by angle θ.

[Start a branch by pushing the current state of the turtle (position and orientation) onto a pushdown stack.

] End a branch by popping a state from the stack and making it the current state of the turtle. No line is drawn, although in general the position of the turtle is changed.

A sample parametric word and its turtle interpretation are shown in Figure 2.

4 The extruded interpretation of L-systems

Turtle interpretation provides a means of visualizing individual elements μ_i of the developmental sequence generated by an L-system $\mathcal{G}$. Although selected structures can be shown side by side, such illustrations fail to convey the continuous aspects of the development of form and pattern over time. To overcome this limitation, we introduce an interpretation of L-systems that represents the entire derivation graph instead of individual strings.

Assume that planar figures $P_0, P_1, \ldots, P_z$ are the structures resulting from the turtle interpretation of the developmental sequence $\mu_0, \mu_1, \ldots, \mu_z$ generated by an L-system $\mathcal{G}$. These structures can be considered to be snapshots of a developmental process, taken at equally spaced points in time $t_0, t_1, \ldots, t_z$, respectively. To visualize this development, we construct an object □, called the *extruded interpretation* of $\mathcal{G}$, such that:

- any cross-section of □ with a plane $t = t_i$ represents figure P_i,
- any cross-section of □ with a plane t such that $t_i < t < t_{i+1}$ (where $i = 0, 1, \ldots, z-1$) is an interpolation between figures P_i and P_{i+1}.

To describe the construction of □ in more detail, we first define the extruded interpretation of individual productions:

- the predecessor and the successor of a production are represented graphically using turtle interpretation,
- the resulting structures are placed in two parallel planes, offset by an interval representing the progress of time,
- selected points (such as vertices) of the predecessor are connected with selected points of the successor to form polygonal faces.

The edges and polygons between the predecessor and the successor can be inserted in many ways. For example, Figure 3 shows two extruded interpretations of the production for the Koch snowflake curve,

$$F(a) \rightarrow F(a/3) + F(a/3) - -F(a/3) + F(a/3). \quad (6)$$

In case (a), each vertex of the successor is connected to the closest endpoint of the predecessor; the midpoint of the successor is connected to both endpoints. In case (b), the three internal vertices of the successor are connected to a "pseudo-vertex" in the middle of the predecessor. In both cases, the extruded objects begin and end with the polygons resulting from the turtle interpretation of the predecessor and the successor. Other cross-sections

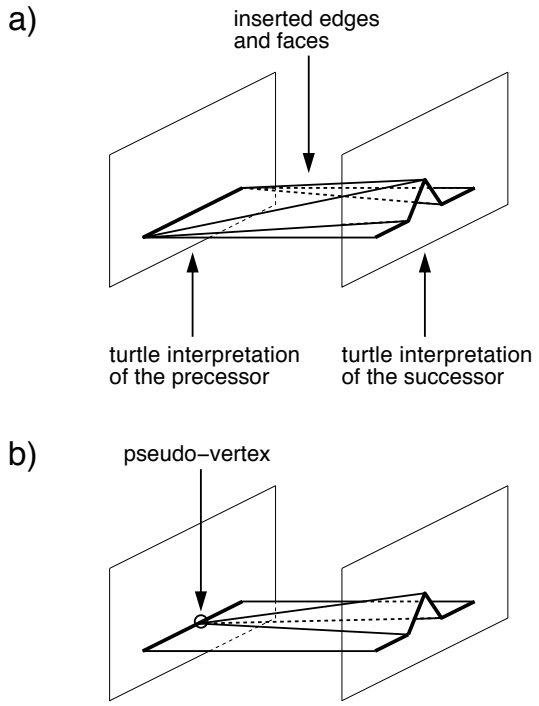

Figure 3: Two extruded interpretations of the production for the Koch snowflake curve (Equation 6)

(perpendicular to the axis of extrusion) represent interpolations between these forms.

Since many interpretations of the same production are possible, our software allows the user to specify the interpretation of each production by assigning an arbitrary graphical procedure to it. The importance of choosing a particular interpolation scheme is not crucial, however, when the differences between the predecessor and successor structures are small, as is the case when productions reflect the progress of time in small intervals. Consequently, we can define the *standard* extruded interpretation of productions, and apply it automatically to any production set.

Consider production p, in which the turtle interpretation of the predecessor is a line segment, and the interpretation of the successor is a non-branching chain of segments. All segments are oriented by the direction in which they are drawn by the turtle. The beginning and end of the predecessor segment are denoted by A_1 and A_2, and consecutive vertices of the successor chain are denoted by $B_1, B_2, \ldots, B_n$ $(n > 1)$, respectively. Let m be equal to $\frac{n}{2}$ if n is even, and $\frac{n+1}{2}$ if n is odd. To form the standard extruded interpretation of the production p, we insert edges between point A_1 and each of the points $B_1, B_2, \ldots, B_m$, as well as between A_2 and each of the points $B_m, B_{m+1}, \ldots, B_n$. Two cases of

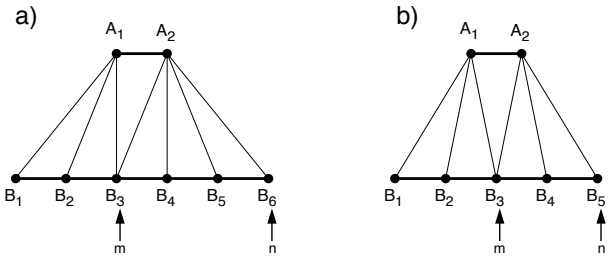

Figure 4: Inserted edges and triangles in the standard extruded interpretation of a production with an even number (a; $n = 6$) and with an odd number (b; $n = 5$) of vertices in the successor segment chain

this construction (for even and odd n) are illustrated in Figure 4. The original segments and the inserted edges bound the sequence of triangles $A_1B_1B_2$, $A_1B_2B_3, \ldots,$ $A_1B_{m-1}B_m$, the triangle $A_1B_mA_2$, and the sequence of triangles $A_2B_mB_{m+1}$, $A_2B_{m+1}B_{m+2}, \ldots, A_2B_{n-1}B_n$. Taken together, these triangles constitute the standard extruded interpretation of the production p. Returning to the Koch snowflake example, Figure 3a shows the standard interpretation of the production used.

In order to handle arbitrary productions, we complement the above definition with the following rules:

- If the predecessor of a production p is not interpreted as a visible line segment (it is an f or a symbol without graphical interpretation), the extruded interpretation of p is empty (it does not contain any inserted edges or polygons).
- If the predecessor of a production p is a visible line, but the successor chain includes invisible line segments (represented by symbols f), only triangles with all edges visible are drawn (Figure 5).
- Branches created by the current production are ignored (Figure 6).

We extend this extruded interpretation from individual productions to derivation steps and then to derivation graphs as follows:

- The extruded interpretation of a derivation step is the union of the interpretations of all productions applied in this step.
- The extruded interpretation of a derivation graph is the union of the interpretations of consecutive derivation steps.

For brevity, the extruded interpretation of the derivation graph generated by an L-system $\mathcal{G}$ is also called the extruded interpretation of $\mathcal{G}$.

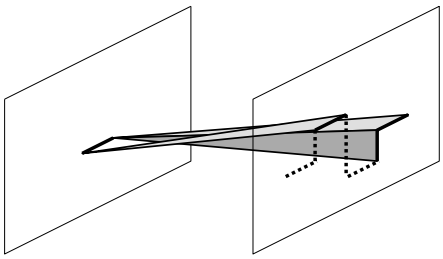

Figure 5: The standard extruded interpretation of a production with invisible line segments (represented by dotted lines) in the successor chain. Triangles bound by invisible edges are not drawn.

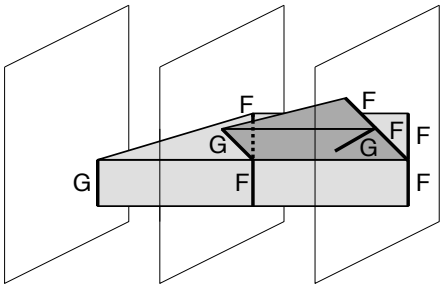

Figure 6: The standard extruded interpretation of two derivation steps generated using an L-system with the production $G \rightarrow F[G]F$. The branching segments created by the current production are ignored, but they are treated as any other segments in the next derivation step.

5 Examples of L-systems with extruded interpretation

The basic idea of the extruded interpretation of L-systems can be illustrated in the simplest way using fractal curves. We consider them in the first two examples and follow with more biologically-oriented models.

5.1 The Koch snowflake curve

The following L-system, presented according to [22], generates the Koch snowflake curve through a gradual progression of shapes.

$$
\begin{array}{lll}
\text{\#define m 10} & \text{/* integer */} & \\
\omega: & F(1,1) & \\
p_1: & F(a,d): \quad a \cong d \quad \rightarrow & \\
 & \quad F\left(\frac{a}{2},\frac{d}{3}\right) + F\left(0,\frac{d}{3}\right) - - & \\
 & \quad F\left(0,\frac{d}{3}\right) + F\left(\frac{a}{2},\frac{d}{3}\right) & \\
p_2: & F(a,d): \quad a > d \quad \rightarrow F\left(a - \frac{d}{2m}, d\right) & \\
p_3: & F(a,d): \quad a < d \quad \rightarrow F\left(a + \frac{d}{m}, d\right) &
\end{array}
\tag{7}
$$

Modules $F(a,d)$ represent line segments, with parameters a and d denoting current and target lengths. The symbol $\cong$ replaces the exact equality $=$ in production p_1 as a reminder that the comparison of parameters a and d should be carried out within the limits of the round-off error, inherent in the floating-point number representation. Modules $+$ and $-$ rotate the turtle by $\pm 60^\circ$.

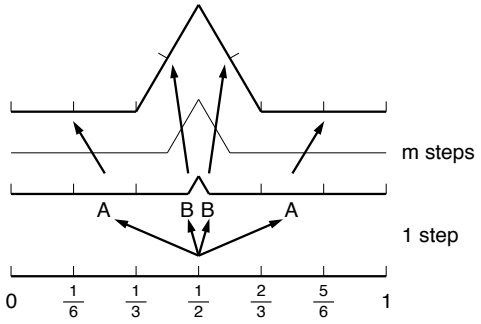

Figure 7: Progression of forms in a continuously developing snowflake curve

In the first derivation step, production p_1 splits the unit-length line $F(1,1)$, specified by the axiom, into four segments labeled **A**, **B**, **B**, **A** in Figure 7. The initial length of segments **A** equals $\frac{1}{2}$, and the initial length of segments **B** equals 0. The target length of all segments is equal to $\frac{1}{3}$. Subsequently, production p_2 decreases the length of each segment **A** by $\frac{d}{2m} = \frac{1}{6m}$ per step, while production p_3 increases the length of each segment **B** by $\frac{d}{m} = \frac{1}{3m}$. Thus, all segments reach simultaneously the same length of $\frac{1}{3}$ after m steps. These segments then subdivide again, and the whole process repeats recursively.

The standard extruded interpretation of L-system (7) for $m = 10$ and the total number of derivation steps $z = 27$ is shown in Plate 1. Notice that all faces of the extruded object have well delineated, straight edges. This fact attracts attention to the discontinuities in the *growth rates* of segments, which occur when the existing segments subdivide and new segments are created.

5.2 A combination of islands and lakes

In [12, page 121], Mandelbrot defined a disconnected fractal, which he called a "combination of lakes and islands". The construction of this fractal is explained in Figure 8. A production subdivides line segments of length d into 6 equal sub-segments and gives rise to two isolated points, which represent degenerate rectangles. Each rectangle is connected to the parent segment by an invisible branch. The rectangles grow during the subsequent m derivation steps, until their shorter and longer edges reach respectively the lengths of $\frac{d}{6}$ and $\frac{d}{3}$. The process of dividing the edges, initiating new rectangles, and growing them is recursively repeated for each of the resulting 18 sub-segments of length $\frac{d}{6}$.

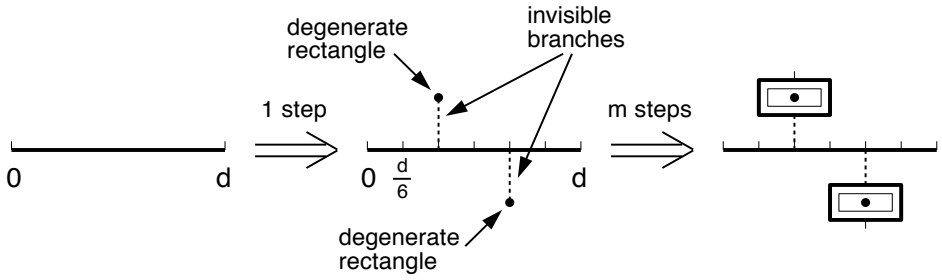

Figure 8: Progression of forms in a continuously developing "combination of islands and lakes"

The standard extruded representation of the described developmental process is shown in Plate 2. Notice that this extruded object was constructed using rules for handling branches and invisible edges.

5.3 A recursively compound leaf

Visualization of biological development is a particularly important practical application of the proposed technique. The following L-system, adapted from [23, Section 6.2.2] models the growth of a recursively compound leaf.

$$
\begin{array}{ll}
\omega: & F_a(0,0) \\
p_1: & F_a(l,t) : t + \Box t < \alpha \rightarrow \\
 & \quad F_a(g_a(t+\Box t), t+\Box t) \\
p_2: & F_a(l,t) : t + \Box t \cong \alpha \rightarrow \\
 & \quad F_b(g_b(0),0) \\
p_3: & F_b(l,t) : t + \Box t < \beta \rightarrow \\
 & \quad F_b(g_b(t+\Box t), t+\Box t) \\
p_4: & F_b(l,t) : t + \Box t \cong \beta \rightarrow \\
 & \quad F_s(g_s(0),0)[+F_a(0,0)][-F_a(0,0)] \\
 & \quad F_b(g_b(0),0) \\
p_5: & F_s(l,t) \rightarrow F_s(g_s(t+\Box t), t+\Box t)
\end{array}
\tag{8}
$$

All modules are interpreted as line segments. Parameter l represents the length of the line, and parameter t indicates the age of the module. The relationship between the age and the length is expressed using growth functions g_a, g_b, and g_s defined further down.

The simulation begins with a segment F_a, which represents a juvenile apex. Its elongation is described by production p_1. When F_a reaches the threshold age of α, production p_2 transforms it into a mature apex F_b[1]. The subsequent elongation of F_b is captured by production p_3. Upon reaching the age of β, F_b divides into an internode F_s, two branches with juvenile apices F_a, and an apex F_b with the initial age of zero (production p_4). All apices then reiterate the developmental pattern described above. Meanwhile, the internodes F_s elongate according to production p_5.

The growth functions must be properly chosen to capture continuous development. We have assumed that the mature apices and the internodes elongate exponentially:

$$
\begin{array}{rcl}
g_b(t) & = & A_b e^{B_b t}, \\
g_s(t) & = & A_s e^{B_s t}.
\end{array}
\tag{9}
$$

In contrast, the development of juvenile apices is expressed by a polynomial function of time, which allows the initial length to be set to zero:

$$
g_a(t) = A_a t^3 + B_a t^2 + C_a t + D_a. \tag{10}
$$

Section 6.2.2 of reference [23] contains a detailed discussion of the relationships that the constants in Equations (9) and (10) must satisfy to produce a model in which the lengths of all branch axes (sequences of internodes terminated by an apex) are first-order continuous functions of time. Consistent with this discussion, the following values were incorporated into L-system (8) to produce the extruded object shown in Plate 3: $\alpha = \beta = 1$, $A_a = -1.52$, $B_a = 2.52$, $C_a = D_a = 0$, $A_b = 1$, $B_b = 0.48$, $A_s = 0.616$, $B_s = 0.48$. The first-order continuity of leaf development is clearly represented by the curves traced by the apices of all branches, which show no sudden changes in slope.

5.4 Pinnate leaf

A pinnate leaf is a compound leaf composed of a main stem (*rachis*) which supports a number of smaller leaflets. The L-system presented below has been adapted from [21], for a more detailed model based on the same principle see [24].

$$
\begin{array}{ll}
\omega: & F_a(l_0, n_0) \\
p_1: & F_a(l,n) : l < l_{th} \rightarrow \\
 & \quad F_a(l + g(l, r_l, l_{amax})\Box t, n) \\
p_2: & F_a(l,n) : l \geq l_{th} \;\&\; n > 0 \rightarrow \\
 & \quad F_i(kl)[+(\alpha_0)L(s_0)][-(\alpha_0)L(s_0)] \\
 & \quad F_a((1-k)l, n-1) \\
p_3: & F_a(l,n) : l \geq l_{th} \;\&\; n = 0 \rightarrow \\
 & \quad F_i(l)L(s_0)
\end{array}
\tag{11}
$$

[1] It is assumed for simplicity that the threshold age values α and β are integer multiples of the time increment $\Box t$. Methods for eliminating this assumption are discussed in [7].

$$
\begin{array}{lll}
p_4: & F_i(l) & \rightarrow F_i(l + g(l, r_i, l_{imax})\Box t) \\
p_5: & L(s) & \rightarrow L(s + g(s, r_s, s_{max})\Box t) \\
p_6: & \pm(\alpha) & \rightarrow \pm(\alpha + g(\alpha, r_\alpha, \alpha_{max})\Box t)
\end{array}
$$

Development begins with an apex F_a; the associated parameters specify its initial length l_0 and the number of leaflet pairs to be produced n_0. While the length l is less then the threshold value l_{th}, production p_1 increases l according to a logistic growth function [5, 29], which is defined by the differential equation:

$$\frac{dl}{dt} = r_l \left(1 - \frac{l}{l_{amax}}\right) l = g(l, r_l, l_{amax}). \qquad (12)$$

When the length reaches the threshold l_{th}, one of two events can take place. If there are one or more leaflet pairs yet to be produced, the apex is replaced by a branching structure consisting of an internode F_i, two leaflets L within branches, and another apex (production p_2). Alternatively, if n_0 leaflet pairs have already been produced, the apex creates an internode and a terminal leaflet (production p_3). Productions p_4, p_5, and p_6 control further growth of the internodes and leaflets, and the increase of the magnitude of branching angles.

An extruded object illustrating the operation of this L-system is shown in Plate 4. The values of constants used in the simulation are: $n_0 = 4$, $l_0 = 1$, $l_{th} = 2$, $r_a = 2$, $l_{amax} = 3$, $k = 0.5$, $r_i = 1$, $l_{imax} = 3$, $s_0 = 0.05$, $r_s = 2$, $s_{max} = 6$, $\alpha_0 = 2^\circ$, $r_\alpha = 1$, $\alpha_{max} = 60^\circ$. The leaflets are represented as diamond-shaped polygons as described in [23, page 120]. The extruded object clearly shows that the production of consecutive leaflet pairs is offset in time, and that leaflet expansion is faster than the gradual increase of the branching angles that define leaflet position on the rachis ($r_s > r_\alpha$).

6 L-systems and partial differential equations

Interesting applications of parametric context-sensitive L-systems stem from their capability of expressing numerical solutions to initial value problems for partial differential equations. This capability was originally explored in the context of simulations performed using CELIA, the first software implementation of L-systems [1, 2, 8, 11], with the most general observations made in [9]. In this section, we present an approach to solving the initial value problem for PDEs with L-systems, using a parabolic (diffusion) equation as an example. We then apply this approach to solve a system of reaction-diffusion equations operating in a one-dimensional medium of constant size, as well as in an expanding medium. These solutions represent the evolution of the spatial distribution of the dependent variable(s) over time, and therefore lend themselves in a natural way to visualizations using extruded objects in space-time. In the examples considered, the visualizations lead to a realistic image of the shell of *Nautilus pompilius* with a pigmentation pattern, and to a graphical representation of the development of a filamentous bacteria *Anabaena catenula*.

6.1 Diffusion and decay

Let us consider the following equation:

$$\frac{\partial u}{\partial t} = -\nu u + D\frac{\partial^2 u}{\partial x^2}. \qquad (13)$$

If u is interpreted as the concentration of a substance C, this equation represents the decay of C with time constant ν and the diffusion of C along axis x with the diffusion coefficient D (for example, see [5]). Suppose that we want to solve this equation in the interval $[a, b]$ for $t \geq 0$, assuming the boundary conditions $u(a, t) = u_a$, $u(b, t) = u_b$, and the initial conditions

$$u(x, 0) = u_a + (u_b - u_a)\frac{x - a}{b - a}. \qquad (14)$$

Following the finite-difference method [19, Chapter 19], we approximate the derivatives in Equation (13) using values taken at equally spaced sampling points along both the x and t axes:

$$
\begin{array}{rcll}
x_i & = & x_0 + i\Box x, & \text{where } i = 0, 1, \ldots, m, \\
t_j & = & t_0 + j\Box t, & \text{where } j = 0, 1, 2, \ldots.
\end{array} \qquad (15)
$$

Using notation $u_i^j = u(x_i, t_j)$, we obtain:

$$\frac{u_i^{j+1} - u_i^j}{\Box t} = -\nu u_i^j + D\frac{u_{i+1}^j - 2u_i^j + u_{i-1}^j}{(\Box x)^2}, \qquad (16)$$

which leads to

$$u_i^{j+1} = u_i^j + \left(-\nu u_i^j + D\frac{u_{i+1}^j - 2u_i^j + u_{i-1}^j}{(\Box x)^2}\right)\Box t. \qquad (17)$$

For any values of indices i and j, Equation (17) can be regarded as assigning a new value u_i^{j+1} to the variable u_i^j, taking into account the values u_{i+1}^j and u_{i-1}^j at the neighboring sampling points. Any sampling point along the axis x (except for the boundary points) is subject to a similar assignment, thus Equation (17) can be rewritten as the following context-sensitive L-system production:

$$
\begin{array}{l}
M(u_l) < M(u) > M(u_r) \rightarrow \\
\quad M\left(u + (-\nu u + D\frac{u_l - 2u + u_r}{(\Box x)^2})\Box t\right).
\end{array} \qquad (18)
$$

Notice that the L-system notation eliminates the need for index arithmetic. The subscripts in the formal parameter names u_l, u, and u_r are not numbers, but mnemonic descriptors of the left and right neighbors. Similarly,

indices are not needed to distinguish between the "old" and "new" values of variable u at any point in space, because the progress of time is implicit in the notion of a derivation step in an L-system.

To provide a framework for finite differencing expressed by production (18) a complete L-system solving Equation (13) must also:

- create a string of m modules M from the axiom,
- set the initial value of variable u in each module,
- maintain the boundary values of u in the first and the last modules M during the derivation process.

In addition, a graphical output must be associated with each module M if a visual representation of the solution is needed.

Figure 9a shows an extruded representation of the solution to PDE (13) obtained using an L-system in which each module M is shown as a line segment of unit length, with the color dependent on the value of variable u. The values of constants used in this simulation were: $\nu = 0.01, D = 5, a = 0, u_a = 64, b = 128, u_b = 256, \Delta t = 1$, and $m = 128$, yielding $\Delta x = \frac{b-a}{m} = 1$.

6.2 Reaction-diffusion

The described approach to solving partial differential equations using L-systems can easily be extended to systems of equations. In this case, a module M will have several parameters, each representing a different dependent variable. We will illustrate this technique by referring to reaction-diffusion models of the formation of pigmentation patterns in sea shells [6, 14, 15, 16, 17][2]. The models recreate pattern formation in nature, which is characterized by Meinhardt as follows [15, p. vii]:

> A mollusc can enlarge its shell only at the shell margin. In most cases, only at this margin are new elements of the pigmentation pattern added. Therefore, the shell pattern preserves a record in time of a process that took place in a narrow zone at the growing edge. A certain point on the shell represents a certain moment in its history. Like a time machine one can go into the past or the future just by turning the shell back and forth.

[2]The idea of modeling shell patterns using L-systems is not entirely new. Specifically, Baker and Herman generated pigmentation patterns similar to those found in *Oliva porphyria* [2] (see also [9, Chapter 18]) by applying L-systems to express a cellular automaton model proposed by Waddington and Cowe [31]. This approach preceded the formulation of the reaction-diffusion models of pigmentation, first reported in [14], and therefore did not expose the general possibility of expressing reaction-diffusion models using L-systems.

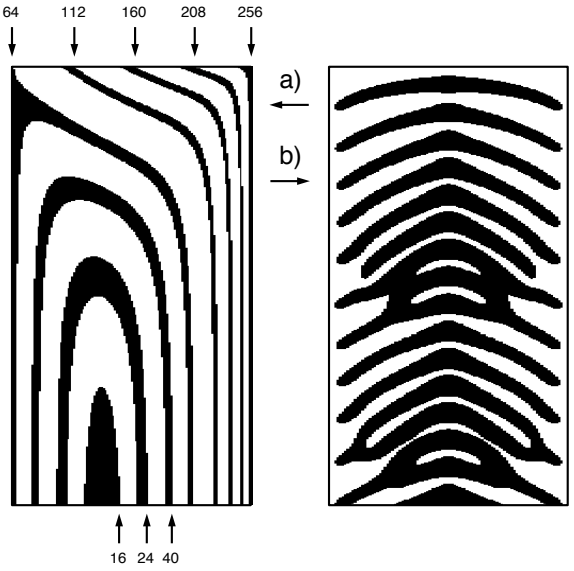

Figure 9: a) Visual representation of a solution to the PDE (13) obtained using an L-system based on production (18). The generated object is a rectangle, with boundaries separating black and white regions indicating the values of variable u. b) Visual representation of a solution to the PDE (19) obtained using an L-system based on production (22). White areas represent concentrations $a < 0.15$, and black areas represent concentrations $a \geq 0.15$. In both figures, time progresses from the top down.

According to this description, a pigmentation pattern can be captured by simulating processes taking place at the growing edge and extruding this edge along an axis representing time. For example, the following system of differential equations was proposed by Meinhardt to model the formation of the pigmentation pattern on the shell of *Nautilus pompilius* [16] (see also [15, page 61]):

$$\begin{aligned} \frac{\partial a}{\partial t} &= a' - \mu a + D_a \frac{\partial^2 a}{\partial x^2}, \\ \frac{\partial s}{\partial t} &= \sigma(x) - a' - \nu s + D_s \frac{\partial^2 s}{\partial x^2}, \end{aligned} \tag{19}$$

where

$$a' = \rho s \frac{a^2}{1 + \kappa a^2} + \rho_0, \tag{20}$$

and

$$\sigma(x) = \sigma_{min} + (\sigma_{max} - \sigma_{min}) \frac{2 \min\{x - x_{min}, x_{max} - x\}}{x_{max} - x_{min}}. \tag{21}$$

The variables a and b in Equation (19) describe concentrations of two chemical substances, called the *activator* and the *substrate*, which diffuse along the growing edge and react with each other. Equation (21) characterizes the production of the substrate $\sigma(x)$ as a triangle-shaped

function of the position of the sampling point x along the edge $[x_{min}, x_{max}]$.

To solve Equation (19) using an L-system, we discretize the growing edge and represent it as a string of modules M. The production that implements the finite difference method is:

$$\begin{aligned} &M(a_l, s_l, \sigma_l) < M(a, s, \sigma) > M(a_r, s_r, \sigma_r) \\ &\quad \rightarrow M\left(a + (a' - \mu a + D_a \tfrac{a_l - 2a + a_r}{(\Delta x)^2})\Delta t,\right. \\ &\quad \left. s + (\sigma - a' - \nu s + D_s \tfrac{s_l - 2s + s_r}{(\Delta x)^2})\Delta t, \sigma\right). \end{aligned} \tag{22}$$

where a' is defined by Equation (20). As in the diffusion-decay example discussed in Section 6.1, the complete L-system for solving Equations (19) must also create the string of modules M and assign the initial and boundary values to the variables. This includes, in particular, the values of substrate production σ, which depend on the module position in the string (Equation 21).

A solution to Equation (19) in the interval

$$[x_{min}, x_{max}] = [0, 100] \tag{23}$$

with the initial conditions $a(x, 0) = s(x, 0) = 0$ and boundary conditions $a(0, t) = a(100, t) = s(0, t) = s(100, t) = 0$, is visualized in Figure 9b. The following constants were used: $\rho = 0.5, \kappa = 1, \rho_0 = 0.004, \mu = 0.1, D_a = 0.1, \nu = 0, D_s = 0.1, \sigma_{min} = 0.012, \sigma_{max} = 0.038, \Delta x = 1$, and $\Delta t = 1$.

The extruded objects depicted in Figures 9a and 9b are planar meshes with different colors assigned to the individual polygons composing the mesh. However, the geometry of the extruded objects can be easily modified, leading to more involved visualizations. For example, a realistic model of the *Nautilus* shell can be obtained assuming that the shell opening has the shape of a circle, growing exponentially from one derivation step to another, and that the axis of extrusion is coiled into a logarithmic spiral (see [6, 15] for details regarding the modeling of shell shape). Both phenomena can be easily expressed using an L-system, resulting in the model shown in Plate 5.

6.3 Reaction-diffusion in an expanding medium

The model of *Nautilus pompilius* extends the range of applications of L-system models to sea shells with pigmentation patterns. More generally, it demonstrates that reaction-diffusion processes can be expressed using L-systems. However, the integration of reaction-diffusion processes and L-systems also leads to a wider class of models of morphogenesis, characterized by reaction-diffusion taking place in expanding media.

From a historical perspective, reaction-diffusion models were originally formulated under the simplifying assumption that the medium in which diffusion takes place does not grow [28]. This assumption dominated subsequent applications of the reaction-diffusion model. Exceptions include the consideration of edge growth in models of the pigmentation pattern of selected sea shells [15, 16], a model of stripe rearrangement during growth on the skin of the fish *Pomacanthus semicirculatus* [10], and a generic model of a growing filament that maintains a constant spacing between dividing and non-dividing cells [3]. In this section we present a related model of the development of the bacteria *Anabaena catenula*.

As described by Mitchison and Wilcox [18], the cells of *Anabaena* are organized into filaments which consist of sequences of *vegetative cells* separated by *heterocysts*. The vegetative cells divide into two cells of unequal length and, in some cases, differentiate into heterocysts which do not further divide. Due to this differentiation, the organism maintains an approximately constant spacing between heterocysts: whenever the distance between two heterocysts becomes too large due to the division and elongation of vegetative cells, a new heterocyst emerges.

What mechanisms is responsible for the differentiation of heterocysts and the maintenance of constant spacing between them? Baker and Herman [1, 2] (see also [4, 8, 11] proposed the following model. The heterocysts fix atmospheric nitrogen and transform it into nitrogenous compounds. These compounds diffuse along the filament and are used by the vegetative cells. When the level of nitrogenous compounds drops below a threshold value, the cells that detect this reduced level differentiate into heterocysts.

Although the model of Baker and Herman is capable of reproducing the observed pattern of heterocyst spacing, it is very sensitive to parameter values. Small changes in these values easily result in filaments with pairs of heterocysts appearing almost simultaneously, close to each other. This is not surprising, considering the operation of the model. The gradient of the concentration of nitrogenous compounds may be too small near the middle of a sequence of vegetative cells to precisely define the point in which a new heterocyst should differentiate. Consequently, the threshold value may be reached almost simultaneously by several neighboring cells, resulting in the differentiation of two or more heterocysts close to each other.

The described model can be improved assuming that the prospective heterocysts compete until one "wins" and suppresses the differentiation of its neighbors. To express this concept, we use the framework of the activator-inhibitor class of reaction-diffusion models [13]. In addition to the nitrogenous compounds that inhibit the differentiation, the cells are assumed to carry a hypothetical substance referred to as the activator. The concentration of the ac-

tivator is the criterion that distinguishes the vegetative cells (low concentration) from the heterocysts (high concentration). The activator and inhibitor are antagonistic substances: the production of the activator is suppressed by the inhibitor unless the concentration of the inhibitor is low. In that case, production of the activator drastically increases through an autocatalytic process (an increased concentration of the activator promotes its own further production). High concentration of the activator also promotes the production of the inhibitor, which diffuses to the neighboring cells. This establishes a ground for competition in which activator-producing cells attempt to suppress production of the activator in the neighboring cells. For proper values of parameters that control this process, only individual, widely spaced cells are able to maintain the high-activation state.

$$
\begin{array}{ll}
\omega: & M(0.5,1,200,\text{right})M(0.5,1,100,\text{right}) \\
& M(0.5,1,100,\text{right}) \\
p_1: & M(s_l,a_l,h_l,p_l) < M(s,a,h,p) > \\
& M(s_r,a_r,h_r,p_r): \\
& \quad s < s_{max}\ \&\ a < a_{th} \rightarrow M(s',a',h',p) \\
p_2: & M(s_l,a_l,h_l,p_l) < M(s,a,h,p) > \\
& M(s_r,a_r,h_r,p_r): \\
& \quad s \geq s_{max}\ \&\ a < a_{th}\ \&\ p = \text{left} \rightarrow \\
& \quad M(ks',a',h',\text{left}) \\
& \quad M((1-k)s',a',h',\text{right}) \\
p_3: & M(s_l,a_l,h_l,p_l) < M(s,a,h,p) > \\
& M(s_r,a_r,h_r,p_r): \\
& \quad s \geq s_{max}\ \&\ a < a_{th}\ \&\ p = \text{right} \rightarrow \\
& \quad M((1-k)s',a',h',\text{left}) \\
& \quad M(ks',a',h',\text{right}) \\
p_4: & M(s_l,a_l,h_l,p_l) < M(s,a,h,p) > \\
& M(s_r,a_r,h_r,p_r): \\
& \quad a \geq a_{th} \rightarrow M(s,a',h',p)
\end{array}
\tag{24}
$$

where

$$
\begin{aligned}
s' &= s(1 + r\Box t), \\
a' &= a + \left(\frac{\rho}{s}\left(\frac{a^2}{1+\kappa a^2} + \rho_0\right) - \mu a + \right. \\
&\quad D_a\left(\frac{a_l - a}{\frac{1}{2}(s_l+s)} - \frac{a - a_r}{\frac{1}{2}(s_r+s)}\right) \\
&\quad \left.\frac{2}{\frac{1}{2}(s_l+s_r)+s}\right)\Box t, \\
h' &= h + \left(\sigma + \rho\frac{a^2}{1+\kappa a^2} - \nu h + \right. \\
&\quad D_h\left(\frac{h_l - h}{\frac{1}{2}(s_l+s)} - \frac{h - h_r}{\frac{1}{2}(s_r+s)}\right) \\
&\quad \left.\frac{2}{\frac{1}{2}(s_l+s_r)+s}\right)\Box t.
\end{aligned}
\tag{25}
$$

L-system (24) implements these mechanisms. The cells are specified as modules M, where parameter s stands for cell length, a is the concentration of the activator, h is the concentration of the inhibitor, and p denotes polarity, which plays a role during cell division. All productions are context-sensitive to capture diffusion of the activator and inhibitor. Production p_1 characterizes elongation of vegetative cells ($a < a_{th}$). A cell that reaches the maximumn length of s_{max} divides into two unequal daughter cells, with the lengths controlled by constant $k < 0.5$. The respective positions of the longer and shorter cells depends on the polarity p of the mother cell, as described by productions p_2 and p_3. Increase of the concentration of the activator a to or above the threshold value a_{th} indicates the emergence of a heterocyst. According to production p_4, a heterocyst does not further elongate or divide. Equations (25) govern the exponential elongation of the cells and the activator-inhibitor interactions [13]. Note the form of the expressions capturing diffusion, with the length of individual cells used to specify current distance between the cell centers. This modification of the standard activator-inhibitor model is intended to minimize the error in estimating the diffusion of substances in a growing filament consisting of cells of unequal size.

To visualize this model, we represent cells as rectangles, with the width indicating cell length and the height indicating concentration of the inhibitor. The extruded interpretation of the development of a filament is shown in Plate 6. The parameters used in the simulation were: $\rho = 3, \kappa = 0.001, \rho_0 = 0.001, \mu = 0.05, D_a = 0.003, \nu = 0.15, D_h = 0.9, \rho_1 = 0, a_{th} = 1, k = \frac{1}{3}, s_{max} = 1, s_{th} = 0.57$. In addition to the geometric attributes, color indicates concentration of the activator (white: low concentration characteristic of the vegetative cells, red: high concentration defining the heterocysts). Notice the sharp peak of the activator concentration at the heterocysts and high levels of the inhibitor in the neighboring vegetative cells preventing their differentiation.

7 Conclusions

In this paper we applied the notion of extrusion to represent the development of one- and two-dimensional structures and patterns using objects in three-dimensional space-time. The developmental processes are simulated using L-systems. The boundary representation of the space-time objects is formed on the basis of predecessor-successor relationships specified by L-system productions. Sample applications include the development of fractal curves and compound leaves, growth of sea shells with pigmentation patterns, and development of a filamentous organism. The *Nautilus* and *Anabaena* models reveal a possibility of expressing reaction-diffusion processes using L-systems. In contrast to the original formulation of reaction-diffusion models, limited to media of constant size, L-systems make it possible to consider reaction-diffusion in expanding media as well.

The presented visualization method was motivated by

a need to illustrate developmental models operating in continuous time, such as those presented in [21] and [23, Chapter 6]. A continuity in the progression of forms is the focal feature of these models and was inadequately represented using sequences of developmental stages.

Several ramifications of the extruded interpretation of L-systems require further research.

- In this paper, we have focused on the automatic construction of a polygon-mesh representation of extruded space-time objects. We left open, however, problems related to the rendering of these objects, such as the determination of which colors or normal vectors should be interpolated for shading purposes.
- The extruded interpretation defines an interpolation between consecutive forms generated by an L-system. This interpolation may be useful in animations of development, making it possible to reduce the number of forms generated directly by an L-system (if this generation is a time-consuming process), and providing a means for temporal antialiasing.
- L-systems with extruded interpretation can be regarded as a variant of the generative modeling paradigm [25, 26], using fractal cross-sections. The modeling power of this technique remains to be investigated.
- Is there an elegant method which would make it possible to model sea shells of arbitrary shape using L-systems with extruded interpretation?
- The combination of reaction-diffusion and L-system models, outlined in Sections 6.2 and 6.3, deserves a thorough study aimed at a better understanding of morphogenetic processes in which both the reaction-diffusion and the growth of the medium play an important role.

Acknowledgement

The reported research has been sponsored by research and equipment grants from the Natural Sciences and Engineering Research Council of Canada.

References

[1] R. Baker and G. T. Herman. CELIA — a cellular linear iterative array simulator. In *Proceedings of the Fourth Conference on Applications of Simulation* (9–11 December 1970), pages 64–73, 1970.

[2] R. Baker and G. T. Herman. Simulation of organisms using a developmental model, parts I and II. *Int. J. of Bio-Medical Computing*, 3:201–215 and 251–267, 1972.

[3] J.-P. Boon and A. Noullez. Development, growth, and form in living systems. In H. E. Stanley and N. Ostrowsky, editors, *On growth and form*, pages 174–183. Martinus Nijhoff Publ., Boston, 1986.

[4] C. G. de Koster and A. Lindenmayer. Discrete and continuous models for heterocyst differentiation in growing filaments of blue-green bacteria. *Acta Biotheoretica*, 36:249–273, 1987.

[5] L. Edelstein-Keshet. *Mathematical models in biology*. Random House, New York, 1988.

[6] D. R. Fowler, H. Meinhardt, and P. Prusinkiewicz. Modeling seashells. Proceedings of SIGGRAPH '92 (Chicago, Illinois, July 26–31, 1992), in *Computer Graphics*, 26, 2 (July 1992), pages 379–387, ACM SIGGRAPH, New York, 1992.

[7] M. Hammel. *Simulation and animation of plant development using differential L-systems*. PhD thesis, University of Calgary, Calgary, Alberta, 1996. In preparation.

[8] G. T. Herman and G. Rozenberg. *Developmental systems and languages*. North-Holland, Amsterdam, 1975.

[9] G. T. Herman and G. L. Schiff. Simulation of multigradient models of organisms in the context of L-systems. *Journal of Theoretical Biology*, 54:35–46, 1975.

[10] S. Kondo and R. Asai. A reaction-diffusion wave on the skin of the marine angelfish *Pomacanthus*. *Nature*, 376:765–768, 31 August 1995.

[11] A. Lindenmayer. Adding continuous components to L-systems. In G. Rozenberg and A. Salomaa, editors, *L Systems*, Lecture Notes in Computer Science 15, pages 53–68. Springer-Verlag, Berlin, 1974.

[12] B. B. Mandelbrot. *The fractal geometry of nature*. W. H. Freeman, San Francisco, 1982.

[13] H. Meinhardt. *Models of biological pattern formation*. Academic Press, London, 1982.

[14] H. Meinhardt. Models for positional signalling, the threefold subdivision of segments and the pigmentations pattern of molluscs. *Journal of Embryology and Experimental Morphology*, 83:289–311, 1984.

[15] H. Meinhardt. *The algorithmic beauty of sea shells*. Springer-Verlag, Berlin, 1995.

[16] H. Meinhardt and M. Klinger. A model for pattern formation on the shells of molluscs. *Journal of Theoretical Biology*, 126:63–89, 1987.

[17] H. Meinhardt and M. Klinger. Pattern formation by coupled oscillations: The pigmentation patterns on the shells of molluscs. In *Lecture Notes in Biomathematics*, volume 71, pages 184–198. Springer-Verlag, Berlin, 1987.

[18] G. J. Mitchison and M. Wilcox. Rules governing cell division in *Anabaena*. *Nature*, 239:110–111, 1972.

[19] W. H. Press, S. A. Teukolsky, W. T. Vetterling, and B. P. Flannery. *Numerical recipes in C: The art of scientific computing*. *Second edition*. Cambridge University Press, Cambridge, 1992.

[20] P. Prusinkiewicz. Graphical applications of L-systems. In *Proceedings of Graphics Interface '86 — Vision Interface '86*, pages 247–253, 1986.

[21] P. Prusinkiewicz, M. Hammel, and E. Mjolsness. Animation of plant development. Proceedings of SIGGRAPH 93 (Anaheim, California, August 1–6, 1993). In *Computer Graphics* Proceedings, Annual Conference Series, 1993. ACM SIGGRAPH, New York, 1993, pp. 369–378.

[22] P. Prusinkiewicz and J. Hanan. L-systems: From formalism to programming languages. In G. Rozenberg and A. Salomaa, editors, *Lindenmayer systems: Impacts on theoretical computer science, computer graphics, and developmental biology*, pages 193–211. Springer-Verlag, Berlin, 1992.

[23] P. Prusinkiewicz and A. Lindenmayer. *The algorithmic beauty of plants*. Springer-Verlag, New York, 1990. With J. S. Hanan, F. D. Fracchia, D. R. Fowler, M. J. M. de Boer, and L. Mercer.

[24] P. Prusinkiewicz, W. Remphrey, C. Davidson, and M. Hammel. Modeling the architecture of expanding *Fraxinus pennsylvanica* shoots using L-systems. *Canadian Journal of Botany*, 72:701–714, 1994.

[25] J. M. Snyder. *Generative modeling for computer graphics and CAD*. Academic Press, Boston, 1992.

[26] J. M. Snyder and J. T. Kajiya. Generative modeling: A symbolic system for geometric modeling. Proceedings of SIGGRAPH'92 (Chicago, Illinois, July 26-31, 1992) in *Computer Graphics*, 26, 2 (July 1992), pages 369–378, ACM SIGGRAPH, New York, 1992.

[27] A. L. Szilard and R. E. Quinton. An interpretation for DOL systems by computer graphics. *The Science Terrapin*, 4:8–13, 1979.

[28] A. Turing. The chemical basis of morphogenesis. *Philosophical Transactions of the Royal Society of London B*, 237:37–72, 1952.

[29] P. F. Verhulst. Notice sur la loi que la population suit dans son accroissement. *Correspondance Mathematique et Physique*, 10:113–121, 1838.

[30] J. Vince. *3–D computer animation*. Addison-Wesley, Wokingham, 1992.

[31] C. H. Waddington and J. Cowe. Computer simulations of a molluscan pigmentation pattern. *Journal of Theoretical Biology*, 25:219–225, 1969.

[32] S. Wolfram. *Mathematica: A system for doing mathematics by computer*. Addison-Wesley, Redwood City, 1988.

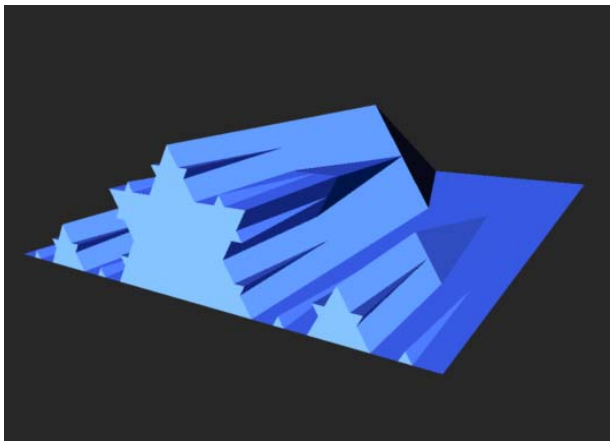

Plate 1: Development of the Koch snowflake curve

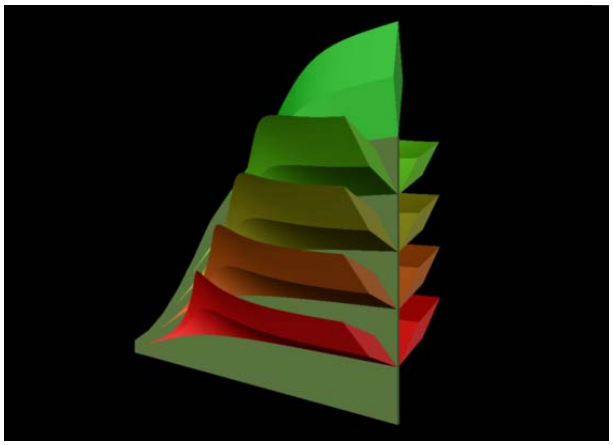

Plate 4: Development of a pinnate leaf

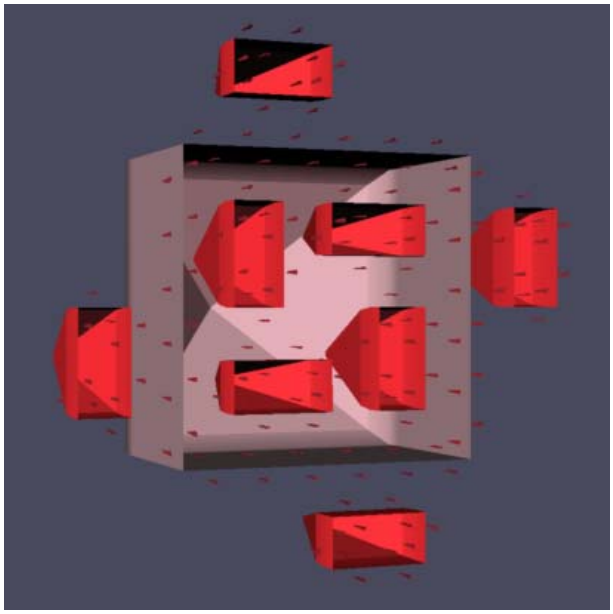

Plate 2: Development of the “islands and lakes” fractal

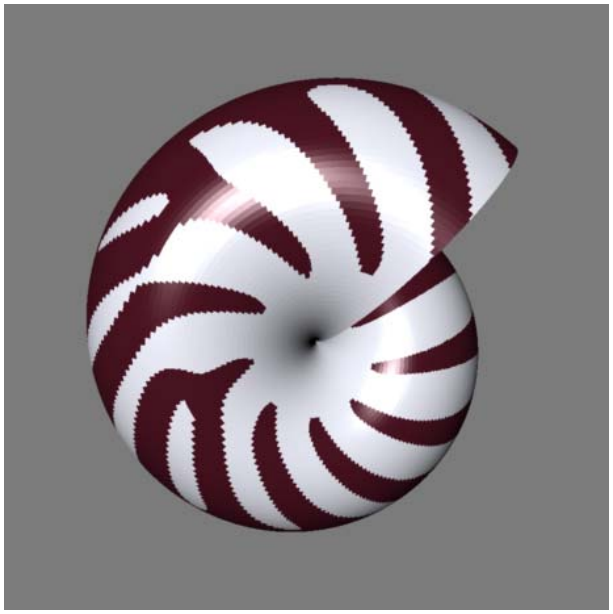

Plate 5: Model of a *Nautilus pompilius* shell

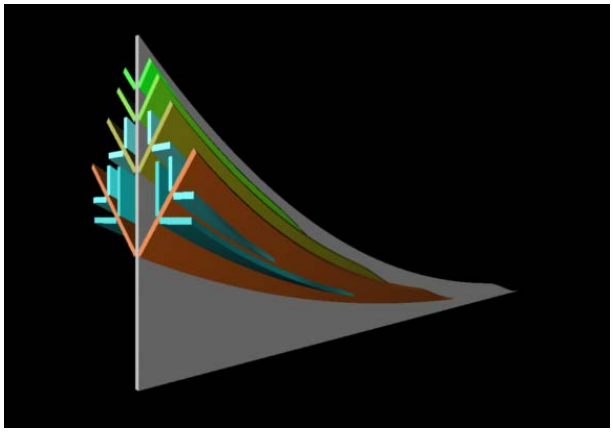

Plate 3: Development of a compound leaf

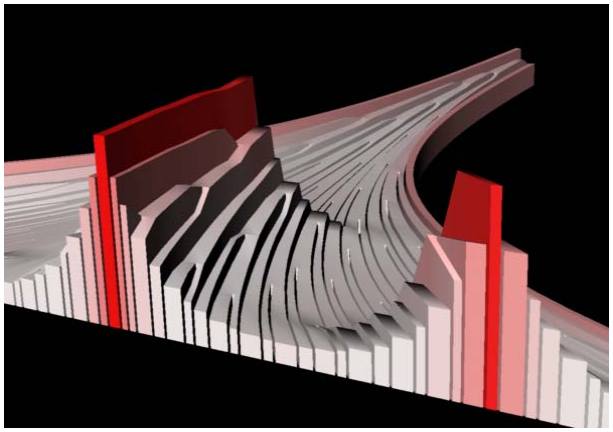

Plate 6: Development of *Anabaena catenula*